Reciprocal Dry Sliding Wear Behaviour of B_4C_p Reinforced Aluminium Alloy Matrix Composites

F. Toptan[a,b,*], I. Kerti[a], L.A. Rocha[b,c]

[a] Yildiz Technical University, Department of Metallurgical and Materials Engineering, Faculty of Chemistry & Metallurgy, Davutpasa Campus, 34210, Esenler, Istanbul, Turkey

[b] Centre for Mechanics and Materials Technologies (CT2M), Universidade do Minho, Azurém, 4800-058 Guimarães, Portugal

[c] Universidade do Minho, Dept. Eng. Mecânica, Azurém, 4800-058 Guimarães, Portugal

* Corresponding author. Tel.: +351 253 510 220; Fax: +351 253 516 007.
E-mail address: ftoptan@dem.uminho.pt (F. Toptan)

ABSTRACT

In the present work, AlSi9Cu3Mg alloy matrix composites reinforced with 15 and 19% (vol.) B_4C_p were produced by squeeze casting route at 850 °C under low vacuum. Titanium-containing flux (K_2TiF_6) was used to promote the wetting between B_4C and liquid aluminium metal. It was found, from the microstructural observations, that the wetting improved by the formation of a thin Ti-rich reaction layer. In order to investigate the wear properties, the samples were subjected to reciprocating wear tests against AISI 4140 pin under dry sliding conditions. Effect of B_4C volume fraction, sliding velocity, applied load and sliding distance on reciprocal dry wear behaviour of composites was studied using general full factorial experimental design. Effects of factors and interactions on the coefficient of friction (COF) and the wear rate values of both composite specimens and counter materials were studied. Worn surfaces and wear debris were characterised using field emission gun scanning electron microscope (FEG-SEM), Energy Dispersive X-Ray Spectroscopy (EDS), optical microscope (OM) and X-Ray diffraction (XRD). From microstructural investigations, wear mechanism suggested as a combination of adhesive, abrasive, and delamination wear.

Keywords: Sliding wear; Metal-matrix composite; Electron microscopy; Wear testing.

1. INTRODUCTION

Particulate reinforced aluminium matrix composites (AMCs) are attractive metal matrix composite (MMC) materials due to their strength, ductility and toughness as well as their ability to be processed by conventional methods [1]. AMCs can be reinforced with various oxides, carbides, nitrides and borides [2-7]. While SiC and Al_2O_3 are the most common reinforcing materials in AMCs, limited research has been conducted on B_4C reinforced AMCs due to the higher cost of B_4C powders [8,9]. However, B_4C is an attractive reinforcement material because of its excellent chemical and thermal stability; most importantly, B_4C has lower density and higher hardness relative to SiC and Al_2O_3 (density values are 2.52, 3.21 and 3.92 g/cm^3 and Knoop Hardness values are 2800, 2480 and 2000, respectively) [8,10-14].

Al-B_4C composites can be processed with low-cost casting routes [3,15-18]. However, in the literature, particle volume fraction values are generally below 15% in cast Al-B_4C composites [15-27]. Relatively higher nominal B_4C volume fractions are used in some works [4,8], however, within this works, there is no information about particle addition yields or actual volume fraction values. It is difficult to obtain high particle addition yields due to the poor wetting between Al and B_4C especially below 1100 °C which makes it difficult to produce Al–B_4C composites by mixing particles into the liquid phase [28]. Apart from wetting, controlling of the interphases occurring at the Al-B_4C interface is also important in the production of cast Al-B_4C composites [29].

It has been reported that the transition metal carbides, borides and nitrides are better wetted than covalently and ionically bonded ceramics [30]. Titanium is one of the reactive metals that can be used to increase wettability in Al-B_4C system [28,31]. Due to the high chemical affinity to boron, titanium easily forms TiC and TiB_2 on the surfaces of boron carbide in Al-B_4C composites and improves wettability as well as particle addition yields. Furthermore, this reaction layer that contains TiC and TiB_2 acts as a "reaction barrier" and limits the undesirable interfacial reactions that can be occurred on the interface. There are some works available in the literature with cast production of Al-B_4C composites with addition of titanium. *Kennedy and Brampton* produced Al-B_4C composites with addition of K-Al-Ti-F flux [28,32]. However, in this works, volume fraction of B_4C particles is maximum 10%.

Besides wetting and particle addition yield, other common problems in cast-AMCs are difficulties of obtaining homogeneous particle distribution and lowering the porosity. The amount of porosity, and its size and distribution are very important in controlling the material's mechanical properties in a cast MMCs. In vortex casting, the vortex sucks air bubbles in the melt resulting in large amounts of porosities in cast MMCs [33,34]. *K. Laden et al.* reported that pores have been created by the vortex during the process and the resulting porosity has been about 5% by volume [35]. On the other hand, increasing particle ratio and decreasing particle size also increase porosity amount in cast MMCs [36,37]. *Mazahery and Shabani* produced A356 matrix B_4C reinforced (5, 7.5, 10, 12.5, and 15 vol.%) composites by squeeze casting route and reported the porosity values as approximately between 0.5 and 2% [26]. In another work, *Canakci and Arslan* produced AA2024 matrix B_4C reinforced (3, 5, 7, 10 vol.%) composites by stir casting route and reported the porosity values as approximately between 2.1 and 3.1% [19].

The dry sliding of AMCs has been widely studied. It is well known that hard ceramic particles improve wear resistance as compared to unreinforced matrix material. The wear rate is related to sliding velocity, particle size, hardness, normal load, chemical composition of the matrix material, particle volume fraction and particle homogeneity [38]. Studies on dry sliding wear in MMCs have been performed with a variety of matrix materials and reinforcements [39]. While SiC and Al_2O_3 reinforced AMCs are the most studied, limited research have been conducted on dry sliding wear of Al-B_4C composites. Generally, pin-on-disc wear test was used in order to study the dry sliding behaviour of Al-B_4C composites [4,20,22,24,25,39,40]. On the other hand, studies on reciprocal dry sliding wear of Al-B_4C composites are very limited and within these studies, contact pressures are relatively high which is higher than the yield strength of matrix alloys [41-43].

Wear behaviour of AMCs are generally investigated by the effect of a single factor, such as sliding distance, sliding speed or contact pressure, on the wear performance. However, the interactions of the factors have certain degree of effects, sometime even strong effects, on the wear behaviour of composites [44]. Several studies are available in the literature on statistical studies of wear behaviour AMCs [44-55], however there is no study available on reciprocal dry sliding wear of Al-B_4C composites.

In the present work, AlSi9Cu3Mg alloy matrix composites reinforced with 15 and 19% (vol.) B_4C_p were produced by squeeze casting route at 850 °C under low vacuum. Titanium-containing flux (K_2TiF_6) was used to overcome the wetting problem between B_4C and liquid aluminium metal. Effects of B_4C volume fraction, sliding velocity, applied load and sliding distance on reciprocal dry wear behaviour of composites were studied using general full factorial experimental design. Effects of factors and interactions on the avg. COF values and wear rate values both in composite specimens and counter materials were studied. Worn surfaces and wear debris were characterised using SEM, EDS, OM and XRD in order to investigate the wear mechanism.

2. EXPERIMENTAL PROCEDURE

2.1. Materials

AlSi9Cu3Mg aluminium alloy was used as matrix material (Table 1) and B_4C particles with an average particle size 32 µm were used as reinforcement. In order to enhance the wettability of B_4C powders and improve their incorporation behaviour into aluminium melts, potassium fluotitanate (K_2TiF_6) flux was used.

Table 1. Chemical composition of AlSi9Cu3Mg matrix material

Al	Si	Fe	Mn	Cr	Ni	Cu	Mg	Pb	Sn	Ti	Zn
82.8	10.14	1.29	0.432	0.021	0. 032	2.99	1.49	0.372	0.008	0.084	0.616

2.2. Composite production

15 and 19% (vol.) B_4C particulate reinforced AMCs were produced in a boron nitride coated graphite crucible utilizing vacuum controlled induction furnace. Mixture of B_4C particles and the K_2TiF_6 flux (with 0.1 Ti/B_4C ratio) were added into the melt at 850°C with mechanical stirring which creates vortex at 1000 rpm. Finally the melt was poured into a metal mould at 900 °C casting temperature and solidified under hydraulic press at 104 MPa. From melting to pouring, process conducted under low vacuum atmosphere at 2.5 mbar.

2.3. Characterisation of as-cast composites

Metallographic samples sectioned from the cast bars were prepared using diamond grinders and water based diamond and colloidal silica suspensions up to 0.04 µm grain size. As-cast microstructures were examined under JEOL JSM 7000F field emission gun scanning electron microscope (FEG-SEM) equipped with Oxford/Inca EDS. Vickers hardness was measured using a Eseway macrohardness tester at a load of 30 Kgf. Volume fraction of particulates were measured by metallographic image analysis technique using Leica ICM 1000 OM and QWin-V 2.8 image analysis software. In order to measure the volume fractions, average 200 measurements was performed in horizontal and perpendicular cross-sections of as-cast composite bars. Experimental volume fraction values are compared with the theoretical volume fraction values and particle addition yield values were calculated.

Density values were measured using Archimedes principle. Density values were calculated with the following formula:

$$\rho = \frac{A}{A-B}(\rho_0 - d) + d \qquad (1)$$

where, ρ is the density of the specimen in g/cm^3, A is the weight in the air in g, B is the weight in the liquid in g, ρ_0 is the density of the liquid in g/cm^3 and d is the density of the air in g/cm^3. Experimental density values are compared with the theoretical density values and % porosity values were calculated.

2.4. Wear Tests

2.4.1. Design of experiments

2^4 full factorial design method was chosen for the design of reciprocating wear testing experiments. Experiments were planned by varying volume fraction, load, sliding velocity and sliding distance. Two levels of each factor were chosen for the study. Volume fraction levels were 15 and 19%, sliding velocity levels were 0.02 and 0.03 m/s, load levels were 20 and 40 N and sliding distance levels were 200 and 400 m. The levels selected for each factor in the design are shown in Table 2. Minitab 15 statistical software was used for designing the experiments. The plan of experiments was prepared by randomising the experiments in order to avoid accumulation of errors. The experiments were conducted based on the randomised run order as given in Table 3. Avg. COF values and wear rate values both in composite specimens and counter materials were taken as responses.

Table 2. Factors and their levels chosen for 2^4 full factorial design

Level	Volume Fraction (%)	Sliding Velocity (m/s)	Load (N)	Sliding Distance (m)
-1	15	0.02	20	200
+1	19	0.03	40	400

Table 3. Plan of experiments

Std Order	Run Order	Factor 1 A: Volume Fraction (%)	Factor 2 B: Velocity (m/s)	Factor 3 C: Load (N)	Factor 4 D: Distance (m)
2	1	19	0.02	20	200
9	2	15	0.02	20	400
12	3	19	0.03	20	400
7	4	15	0.03	40	200
8	5	19	0.03	40	200
14	6	19	0.02	40	400
16	7	19	0.03	40	400
11	8	15	0.03	20	400
1	9	15	0.02	20	200
13	10	15	0.02	40	400
3	11	15	0.03	20	200
5	12	15	0.02	40	200
6	13	19	0.02	40	200
4	14	19	0.03	20	200
10	15	19	0.02	20	400
15	16	15	0.03	40	400

2.4.2. Experimental procedure of wear tests

The wear tests were performed using a PLINT TE 67/R tribometer with a reciprocating plate adapter. Before the wear tests, each specimen polished with the same procedure used for microstructure investigations. Counter materials surfaces were grinded using SiC papers and polished up to 0.04 µm grain size using water based diamond and colloidal silica suspensions. Before starting the wear tests, each specimen was cleaned with propanol in ultrasonic cleaner for ten minutes. The tests were performed against a counter material of an AISI 4140 steel pin with 5 mm diameter in laboratory air conditions. The stroke length was chosen as 10 mm for each test.

After each test, composite samples and pins (counter material) were ultrasonically cleaned for ten minutes and weight loss values were measured using a sensitive balance with an accuracy of 0.1 mg. The formula used to convert the weight loss into wear rate is:

$$W_w = \frac{\Delta W}{s} \tag{2}$$

where W_w is the wear rate in *mg/m*, ΔW is the weight difference of the sample before and after the test in *mg* and S is total sliding distance in *m*.

Finally, wear tracks were examined under FEI Nova 200 FEG-SEM equipped with EDAX, Pegasus X4M EDS/EBSD.

3. RESULTS AND DISCUSSION

3.1. Microstructure of as-cast composites

In order to achieve the desired properties in MMC materials, homogeneous particle distribution should be obtained and wettability of reinforcing materials should be optimized [56]. Relatively homogeneous particle distribution was observed on microstructure of composites as shown in Fig. 1.

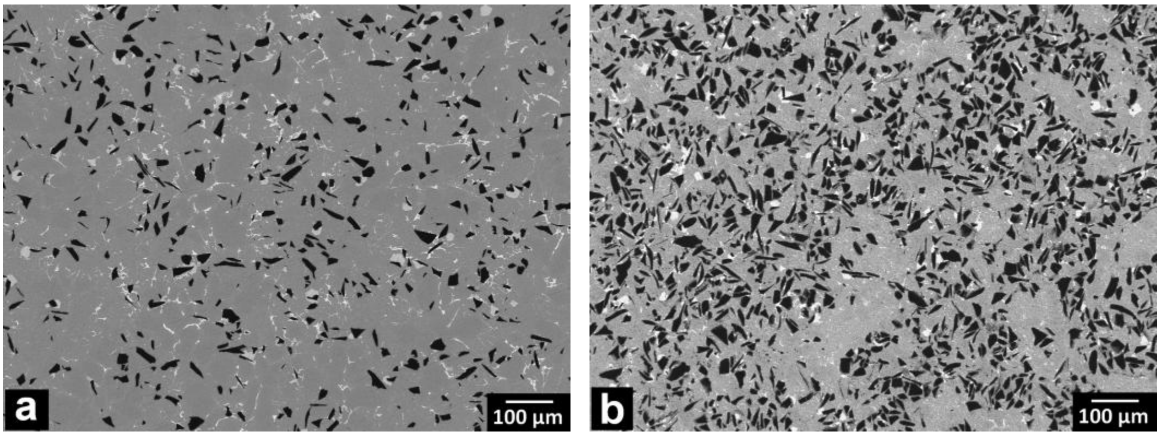

Fig. 1. Back-scattered electron (BSI) SEM images of a) 15% and b) 19% reinforced composites

The potential reactions that could take place in the Al–Ti–B_4C system are reported by *Shen et al*. Since the reaction which produces TiB_2 and TiC has the lowest Gibbs free energy, ΔG, in the Al-Ti-B_4C system, the most favourable reaction products are TiB_2 and TiC in the process temperatures that used in the present work [57]. Fig. 2 shows the SEM images and matching Ti elemental maps for each specimen. As can be seen on the Ti X-ray maps, there are continuous Ti containing layers surrounding B_4C particles which is concluded as consisting of TiB_2 and TiC.

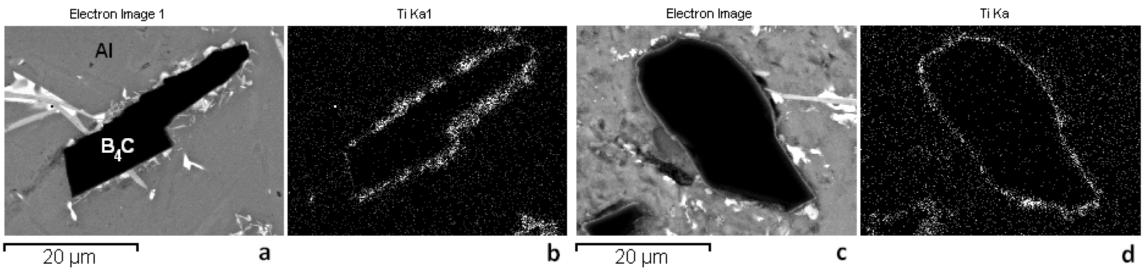

Fig. 2. a, c) BSI SEM images and b,d) matching Ti elemental maps of 15% and b) 19% reinforced composites respectively

Volume fraction (nominal and experimental), particle addition yield and hardness values are given in Table 4. As can be seen from the table, relatively high volume fraction composites produced with 91.54 and 87.02% particle addition yields for 15% and 19% B_4C reinforced composites, respectively. There is very limited information available on the literature related to particle addition yield values in cast-Al-B_4C composites. Due to the low wettability, particle addition yield values are relatively low without any surface modification onto boron carbide particles. *Canakci and Arslan* produced AA2024 matrix B_4C particle reinforced composites by vortex method and reported that, for composites produced with particles between 49-16.5 µm size, particle addition yield is 97% for nominal 3% volume fraction and 65% for nominal 10% fraction [19]. *Kennedy and Brampton* reported 100% approximate yield in composites produced with stir casting using K-Al-Ti-F flux in order to enhance wettability. However, in the study, nominal particle ratio is just 5% (wt.) [28].

Density (theoretical and experimental) and porosity values are also given in Table 4. In the present study, due to the applied vacuum during the process, porosity values are fairly low compared to the literature. For instance, *Mazahery and Shabani* detected approximately 2% porosity in squeeze-cast A356-15% (vol.) composites [26] and *Canakci and Arslan* detected approximately 3% porosity in stir-cast AA2024-10% (vol.) composites [19].

Table 4. Physical properties and hardness values

Specimen	Nominal Volume Fraction (%)	Experimental Volume Fraction (%)	Particle Addition Yield (%)	Theoretical density (g/cm^3)	Experimental density (g/cm^3)	% Porosity	Hardness (HV)
AlSi9Cu3Mg-15%B_4C	16.20	14.83±2.70	91.54	2.75	2.74±0.0108	0.33	119.03±2.68
AlSi9Cu3Mg-19%B_4C	21.50	18.71±5.15	87.02	2.77	2.74±0.0098	1.12	135.15±5.35

3.2. Dry sliding wear behaviour

Table 5 provides the experimental plan and the experimental results for avg. COF values and wear rate values both in composite specimens and counter materials.

Table 5. Experimental plan with results

Std Order	Run Order	Factor 1 A: Volume Fraction (%)	Factor 2 B: Velocity (m/s)	Factor 3 C: Load (N)	Factor 4 D: Distance (m)	Avg. COF	Wear rate (mg/m)	Wear rate of pins (mg/m)
2	1	19	0.02	20	200	0.81±0.10	0.01950	0.0015
9	2	15	0.02	20	400	0.81±0.12	0.02075	0.0033
12	3	19	0.03	20	400	0.86±0.11	0.02350	0.0060
7	4	15	0.03	40	200	0.53±0.04	0.02150	0.0050
8	5	19	0.03	40	200	0.70±0.08	0.02300	0.0095
14	6	19	0.02	40	400	0.80±0.08	0.03650	0.0365
16	7	19	0.03	40	400	0.70±0.06	0.01750	0.0035
11	8	15	0.03	20	400	0.79±0.11	0.01400	0.0033
1	9	15	0.02	20	200	0.74±0.10	0.00650	0.0050
13	10	15	0.02	40	400	0.74±0.08	0.03100	0.0310
3	11	15	0.03	20	200	0.57±0.06	0.02000	0.0080
5	12	15	0.02	40	200	0.48±0.03	0.02450	0.0060
6	13	19	0.02	40	200	0.85±0.08	0.04450	0.0140
4	14	19	0.03	20	200	0.81±0.12	0.02350	0.0040
10	15	19	0.02	20	400	0.98±0.15	0.03125	0.0043
15	16	15	0.03	40	400	0.51±0.04	0.02125	0.0070

3.2.1. Analysis of coefficient of friction values

COF graphs for light wear conditions (run orders 9 and 1 in Table 3 for 15% and 19% reinforced composites, respectively) and harsh wear conditions (run orders 16 and 7 in Table 3 for 15% and 19% reinforced composites, respectively) are given in Fig. 3. Similar trends were observed for the other conditions but with different average COF values. The average COF values are in the range of 0.48 and 0.98. In all conditions, COF values of 19% B_4C reinforced composites were higher than 15% B_4C reinforced composites. Furthermore, COF values are almost linearly increased during sliding distance.

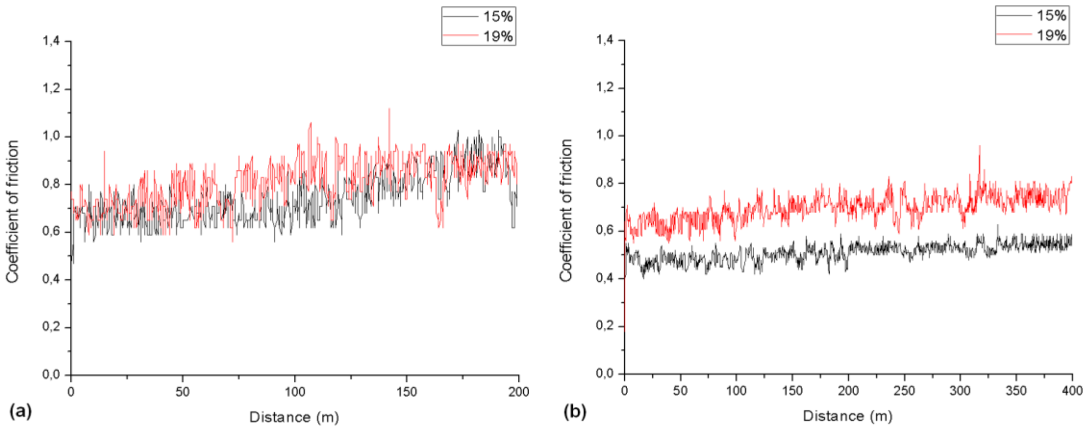

Fig. 3. COF graphs for a) light and b) harsh wear conditions

The COF values were statistically investigated using Minitab 15 statistical software. Fig. 4 (a) shows the normal probability plot for avg. COF values. As can be seen on the graph, avg. COF values are reasonably fitted to normal distribution. Fig. 4 (b) shows the main effect plots for avg. COF values. Avg. COF values are increased with volume fraction and sliding distance and decreased with sliding velocity and normal load.

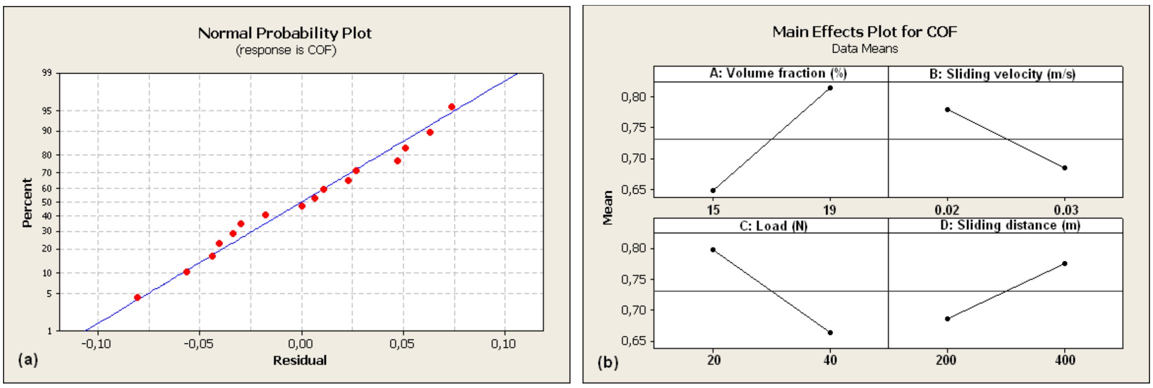

Fig. 4. a) Normal probability and b) main effect plots for avg. COF

Table 6 shows the results of the analysis of variance (ANOVA) table with the avg. COF values. ANOVA table shows source, degree of freedom (DF), sum of squares (SS), mean squares (MS), F value and percentage of contribution (P%). In the present work, only double interactions are investigated for all responses and level of confidence is chosen as 95%. The last column of the table shows the percentage of contribution, P (%), of each factor on the total variation indicating the degree of influence on the result. Percentage of contribution is calculated using the following formula [58,59]:

$$P(\%) = \frac{SS_F}{SS_T} \times 100 \tag{3}$$

where, SS_F is sum of squares of the factors or the interactions and SS_T is total sum of squares. The factors and the interactions which have bigger F value than $F_{\alpha=5\%}$ and bigger P (%) value than the P (%) value of the error associated are taken as statistically and physically significant factors and interactions [58].

Analysis of the ANOVA table for avg. COF values (Table 6) showed that volume fraction (P = 36.41%) presented the strongest statistical and physical significance on the avg. COF values, followed by load (P = 23.81%). Other factors and interactions do not present statistical significance on the avg. COF values within the confidence level chosen.

Table 6. ANOVA table for avg. COF

Source†	DF	SS	MS	F	P (%)
A	1	0.1110110	0.1110110	17.79	36.41
B	1	0.0361430	0.0361430	5.79	11.86
C	1	0.0725760	0.0725760	11.63	23.81
D	1	0.0324050	0.0324050	5.19	10.63
A*B	1	0.0000050	0.0000050	0.00	0.00
A*C	1	0.0037830	0.0037830	0.61	1.24
A*D	1	0.0078090	0.0078090	1.25	2.56
B*C	1	0.0009330	0.0009330	0.15	0.31
B*D	1	0.0022490	0.0022490	0.36	0.74
C*D	1	0.0067420	0.0067420	1.08	2.21
Error	5	0.0311950	0.0062390		10.23
Total	15	0.3048520			100

†A: Volume fraction (%); B: Sliding velocity (m/s); C: Load (N); D: Sliding distance (m)

In the literature, testing conditions for dry sliding of Al-B_4C composites are not similar with the present work. Particularly, for reciprocal sliding of Al-B_4C composites, contact pressures are much higher than the present study and the type and/or geometry of the counter material is different. In the present work, contact pressures are 1.02 and 2.04 MPa for 20 N and 40 N normal loads, respectively. *Meydanoglu et al.* studied reciprocal dry sliding of hot pressed Al-B_4C (10% wt.) composites against Al_2O_3 ball with 10mm diameter with 100 g load, 0.02 and 0.09 m/s sliding velocity and 120 m sliding distance. The authors obtained different COF values with average particle size and sliding velocity. For 10 µm B_4C reinforced composites, avg. COF values are 0.93±0.04 and 0.69±0.11 and for 25 µm B_4C reinforced composites, the values are 1.10±0.04 and 0.89±0.13 against 0.02 and 0.09 m/s sliding velocity, respectively [41]. *Hemanth* studied unidirectional (pin-on-disc) dry sliding wear of Al–12% Si matrix B_4C_p reinforced (3 to 12 vol.% insteps of 3 vol.%) composites produced by vortex. The author used oil quenched SCM 4 (equivalent to AISI 4140) counter material, three different loads (10, 20 and 30 N), six sliding speeds (0.3–1.8 insteps of 0.3 m/s) and constant sliding distance (3000 m). As a comparison with the present study; the author measured 0.7 COF value for 12% reinforced composite under 0.03 m/s sliding velocity and 30 N normal load [20]. In the present study, with 15% particle volume fraction, 0.03 m/s sliding velocity and 20 N normal load (corresponds to similar contact pressure), 0.57 and 0.79 avg. COF values measured for 200 and 400 m sliding distances, respectively.

3.2.2. Analysis of wear rate values of specimens

Normal probability plot of wear rate values of specimens are given in Fig. 5 (a). As can be seen on the graph, values are reasonably fitted to normal distribution. Fig. 5 (b) shows the main effect plots for wear rate values. Wear rate values increased with volume fraction, load and sliding distance and decreased with sliding velocity.

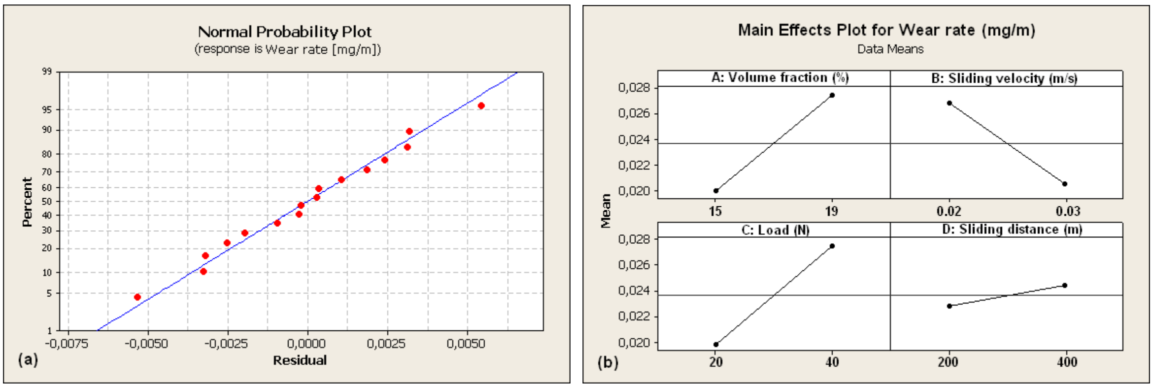

Fig. 5. a) Normal probability and b) main effect plots for wear rate

Analysis of the ANOVA table for the wear rate values (Table 7) showed that load (P = 19.43%) presented the strongest statistical and physical significance on the wear rate values, followed by volume fraction (P = 18.79%). B*C interaction (sliding velocity*load) also presented statistical and physical significance on the wear rate values (P = 16.66%). Other factors and interactions do not present statistical significance on the wear rate values within the confidence level chosen.

Table 7. ANOVA table for wear rate

Source†	DF	SS	MS	F	P (%)
A	1	0.0002231	0.0002231	9.28	18.79
B	1	0.0001578	0.0001578	6.56	13.29
C	1	0.0002307	0.0002307	9.59	19.43
D	1	0.0000102	0.0000102	0.42	0.86
A*B	1	0.0000914	0.0000914	3.80	7.70
A*C	1	0.0000110	0.0000110	0.46	0.93
A*D	1	0.0000165	0.0000165	0.69	1.39
B*C	1	0.0001978	0.0001978	8.22	16.66
B*D	1	0.0000821	0.0000821	3.42	6.92
C*D	1	0.0000464	0.0000464	1.93	3.91
Error	5	0.0001202	0.0000240		10.12
Total	15	0.0011872			100

†A: Volume fraction (%); B: Sliding velocity (m/s); C: Load (N); D: Sliding distance (m)

It is generally accepted that during the dry sliding of AMCs, as normal load increases the wear rate also increases. It is also expected that if particle volume fraction increases the wear rate decreases. However, statistical analysis showed that there is an increase on the wear rate values with the increment of the volume fraction.

As it is given in Table 4, the porosity values of AlSi9Cu3Mg-19%B_4C composite is higher than AlSi9Cu3Mg-15%B_4C. Besides, hardness of the 19% reinforced composite is not as higher as expected than the 15% reinforced composite. It was concluded that this small difference on the hardness value is mainly due to the higher porosity of the 19% reinforced composite. Furthermore, due to the higher porosity, the subsurface cracks may connect easier in 19% reinforced composites as compared to the 15% composites. Hence, the amount of removing particles can be expected more in the 19% reinforced composites than the 15% composites. Therefore, due to the third body effect of those particles, the wear rate of the 19% reinforced composite is higher than the 15% reinforced composite. However, it is concluded that the third body effect is not dominant on the wear mechanism. It is observed from the microstructures that, the huge amounts of the reinforcing particles are still intact on the surface after sliding. It should be underlined that, due to the extremely higher hardness of the B_4C particles, under dominant third body effect conditions, the increment on the wear rate values can be expected to increase dramatically which did not observed in the present system.

3.2.4. Analysis of wear rate values of counter materials

Normal probability plot of wear rate values in counter material are given in Fig. 6 (a). As can be seen on the graph, values are reasonably fitted to normal distribution. Fig. 6 (b) shows the main effect plots for wear rate by weight loss values in counter material. Wear rate values increased with volume fraction, load and sliding distance and decreased with sliding velocity. The main effects of factors generally showed the same tendency with wear rate values in samples but with different percentages.

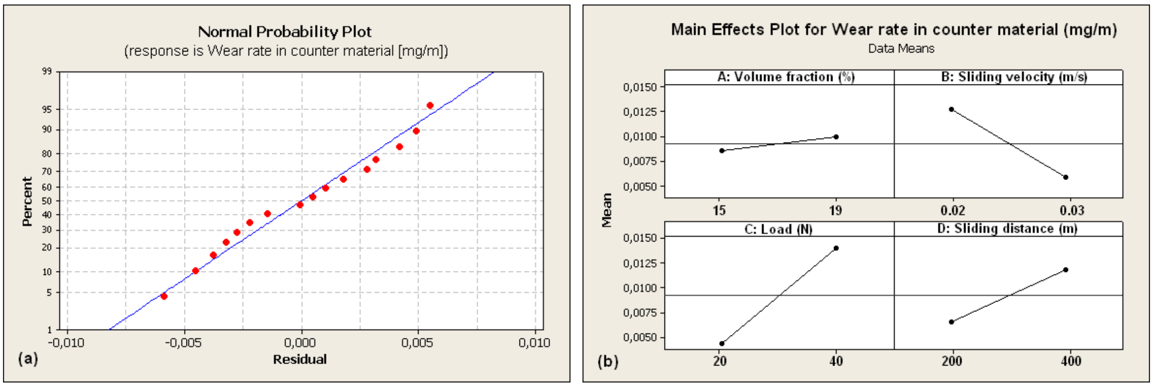

Fig. 6. Normal probability and b) main effect plots for wear rate in counter material

Analysis of the ANOVA table for the wear rate values in counter materials (Table 8) showed that load (P = 24.54%) presented the strongest statistical and physical significance on the wear rate values, followed by B*C (sliding velocity*load) interaction (P = 20.01%). Other factors and interactions do not present statistical significance on the wear rate values in counter material within the confidence level chosen.

Table 8. ANOVA table for wear rate values in counter material

Source†	DF	SS	MS	F	P (%)
A	1	0.0000072	0.0000072	0.19	0.47
B	1	0.0001908	0.0001908	5.07	12.55
C	1	0.0003730	0.0003730	9.90	24.54
D	1	0.0001089	0.0001089	2.89	7.17
A*B	1	0.0000079	0.0000079	0.21	0.52
A*C	1	0.0000208	0.0000208	0.55	1.37
A*D	1	0.0000000	0.0000000	0.00	0.00
B*C	1	0.0003041	0.0003041	8.07	20.01
B*D	1	0.0001908	0.0001908	5.07	12.55
C*D	1	0.0001280	0.0001280	3.40	8.42
Error	5	0.0001883	0.0000377		12.39
Total	15	0.0015198			100

†A: Volume fraction (%); B: Sliding velocity (m/s); C: Load (N); D: Sliding distance (m)

When the wear rate values in composite specimens and counter materials are compared, it can be seen that load is the most significant factor and B*C (sliding velocity*load) is the most significant interaction in both case with different percentage of contributions. However, while volume fraction factor is statistically significant on the wear rate of composite specimens, it does not present statistical significance on the wear rate values in counter materials.

3.2.5. Microstructural analysis of the worn surfaces

Microstructure of the worn surfaces of composite specimens and matching counter materials' surfaces are investigated using OM and SEM for light and harsh wear conditions. The morphology of the worn surface of composite specimens shown in low magnification SEM images in Fig. 7. Parallel sliding marks along the sliding direction are visible on the worn surfaces for both volume fraction and both conditions. However, 19% reinforced composites have relatively smooth surface for both conditions. Matching EDS analysis results are also given in Fig. 7. As can be seen on the EDS spectrums, presence of Fe and O is detected for all conditions which prove that there is a material transfer from counter material and that transferred material probably oxidised during the sliding.

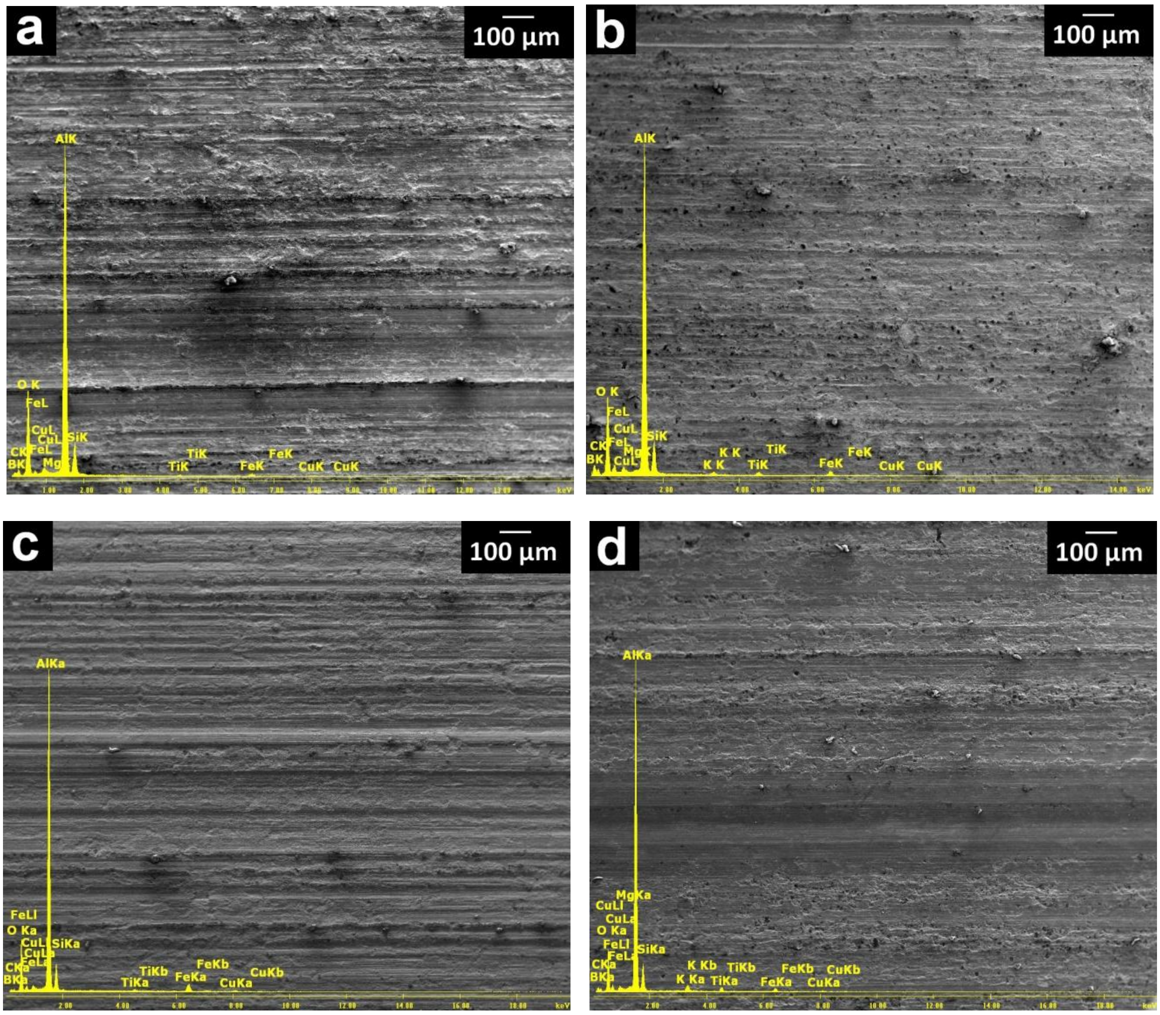

Fig. 7. Low magnification secondary electron (SE) SEM images of the worn surfaces and matching EDS analysis for a) 15%, b) 19% reinforced composites worn in light conditions and c) 15%, d) 19% reinforced composites worn in harsh conditions

In higher magnification examinations, the worn surfaces showed following features: (i) grooves, (ii) protrusions, (iii), craters, (iv) flakes, (v) iron on worn surface, (vi) oxide on worn surface, (vii) plastic deformation, (viii) cracks, and (ix) heap of loose debris. While grooves and Fe and O on the worn surfaces are common in both volume fractions and conditions, other features are observed in some conditions.

Fig. 8 shows the B_4C protrusions on the worn surface of 15% B_4C reinforced composite worn in light conditions. Those protrusions only observed in light conditions. In harsh conditions, they probably get flat or covered with wear debris.

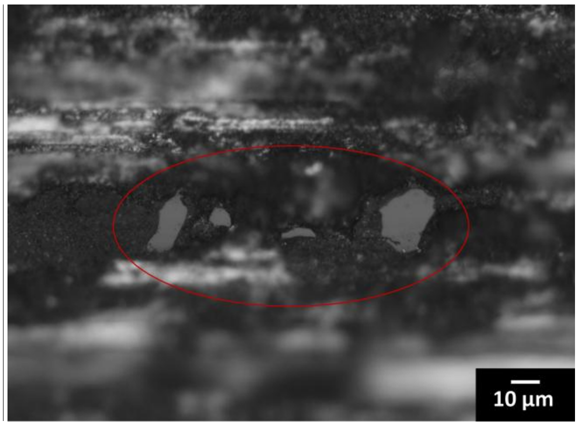

Fig. 8. OM image showing B_4C protrusions on the worn surface of 15% reinforced composite worn in light conditions

Fig. 9 shows the craters on the worn surface of 19% B_4C reinforced composite worn in harsh conditions. It has been reported that, detached layer in the form of craters or cavities indicates locally adhesive wear due to the formation of and breaking of micro welds during sliding [24].

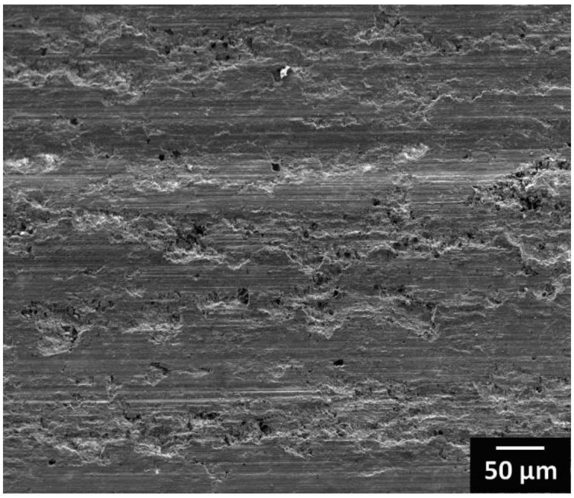

Fig. 9. SE SEM image of the craters on the worn surface of 19% B_4C reinforced composite worn in harsh conditions

Fig. 10 shows SEM image of a large flaky piece which is about to be dislodged from the surface. The EDS analysis taken from the marked area in Fig. 10 (a) shows that the flake contains Al, Fe (from counter material) and oxides (Fig. 10 (b)).

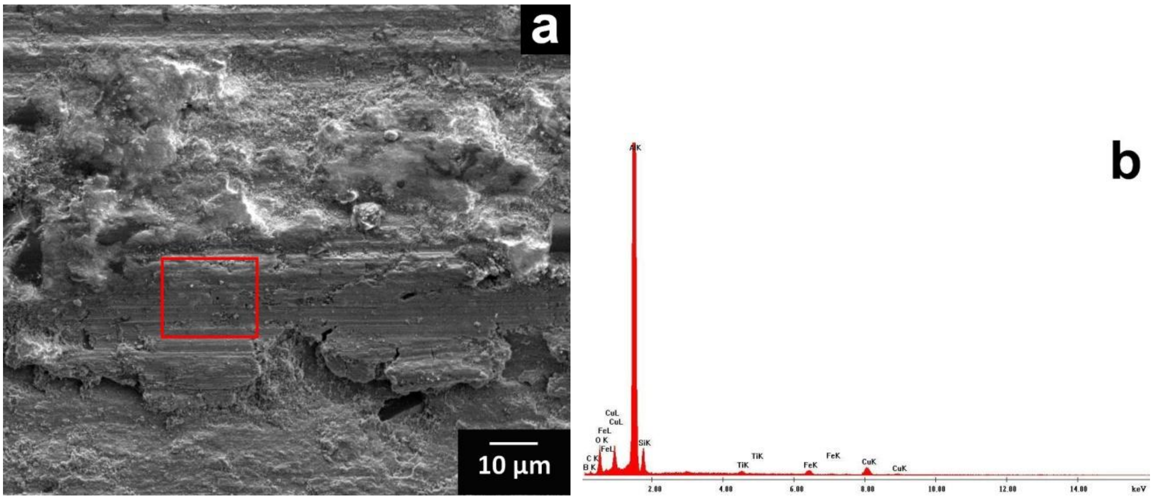

Fig. 10. a) SE SEM images of a large flaky piece is about to be dislodged from the surface from 15% B_4C reinforced composite worn in light conditions and b) EDS analysis taken from the marked area

It has been reported that, for microstructures containing hard second-phase particles, if sufficient plastic deformation occurred during sliding wear, crack nucleation was favoured at these particles. In this case, inter-particle spacing is an important variable and crack propagation controlled the wear rate. Void formation was primarily attributed to the plastic flow of the matrix metal around these hard second-phase particles. Void formation occurred very readily around the particles but crack propagation occurred very slowly. The depth at which the void nucleation was initiated and the void size tended to increase with increased COF and applied load [60]. Plastic deformation and cracks related to delamination wear were observed on worn surfaces. However, delamination wear is not the dominant wear mechanism in all cases that studied. Fig. 11 (a) shows the plastic deformation traces and Fig. 11 (b) shows the cracks on the worn surfaces.

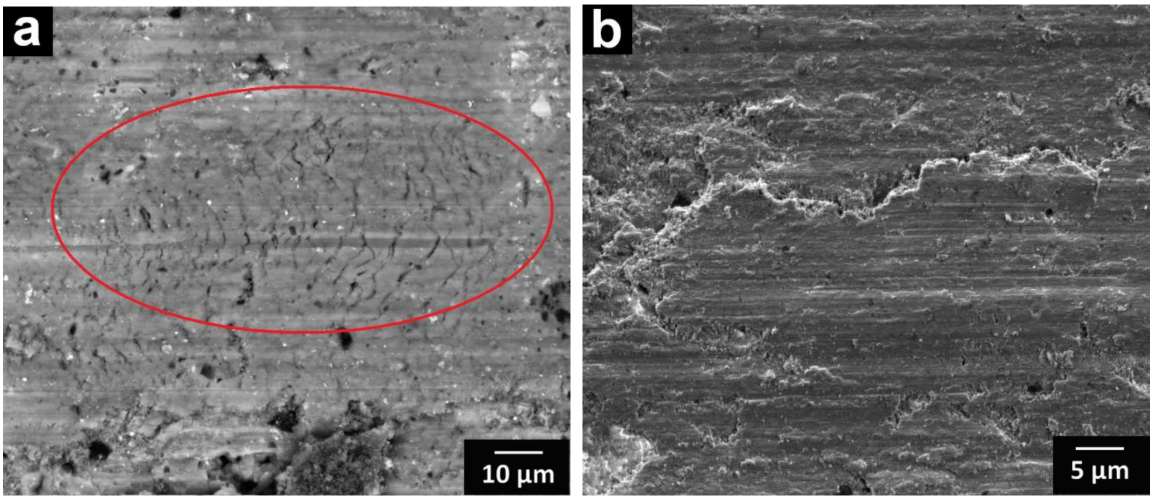

Fig. 11. Plastic deformation on a) 15% reinforced composite worn in light conditions and b) cracks on 19% reinforced composite worn in harsh conditions in BSI and SE SEM images, respectively

Fig. 12 shows SEM image of uncompacted powdery debris contains Al, Fe and oxides that confirmed with the EDS analysis taken from the same area. It has been reported that the loose wear debris has the same structure and composition as the transferred layer [60]. Therefore, together with COF values it has concluded that a tribolayer containing Fe, Al and oxides formed during the sliding on the surfaces of composite specimens. Same features (large flaky piece and uncompacted powdery debris) were observed by *Shorowordi et al.* worked with unidirectional dry sliding of Al-13% B_4C_p composites against a commercial phenolic brake pad [22].

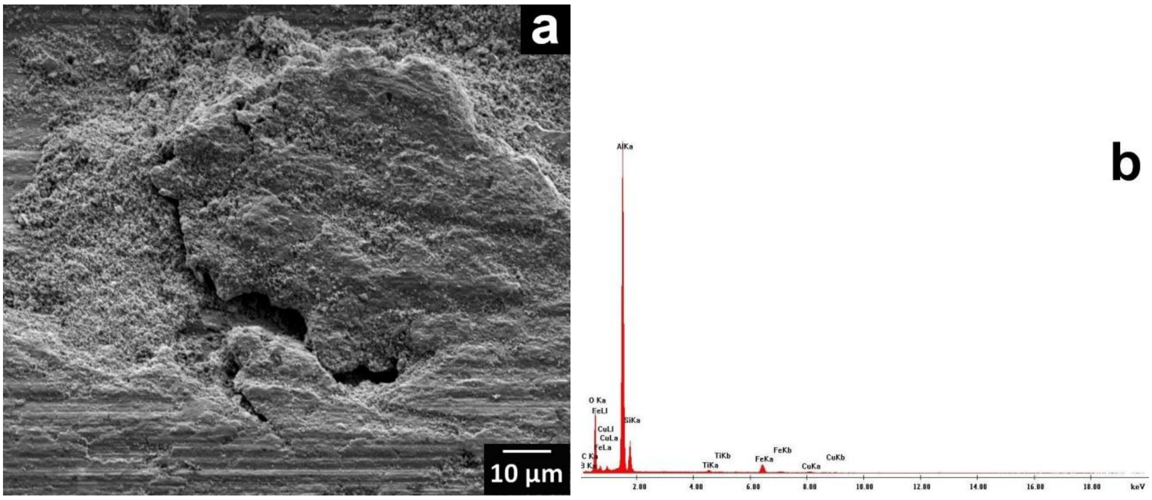

Fig. 12. a) SE SEM image and b) matching EDS analysis of uncompacted powdery debris from 19% B_4C reinforced composite worn in harsh conditions

Surfaces of pins (counter material) were also investigated with SEM and EDS. Low magnification SEM images are given in Fig. 13. It is visible on the images that pins have parallel sliding marks along the sliding direction on the worn surfaces for both volume fraction and both conditions. However, grooves are shallower compared to composite worn surfaces. In addition to grooves, some dark regions and patches can be seen on the worn surfaces of pins. Since the images are taken on BSI mode, these regions appear to contain Al or oxides. Matching EDS analysis results taken from the images are also given in Fig. 13 confirm that worn surfaces of pins contains relatively high amounts of Al and O. Furthermore, analysis also contains C in pins worn again 15% B_4C reinforced composites and both B and C in pins worn against 19% B_4C reinforced composites means that there is also reinforcing material transfer from composite materials to pins during the sliding.

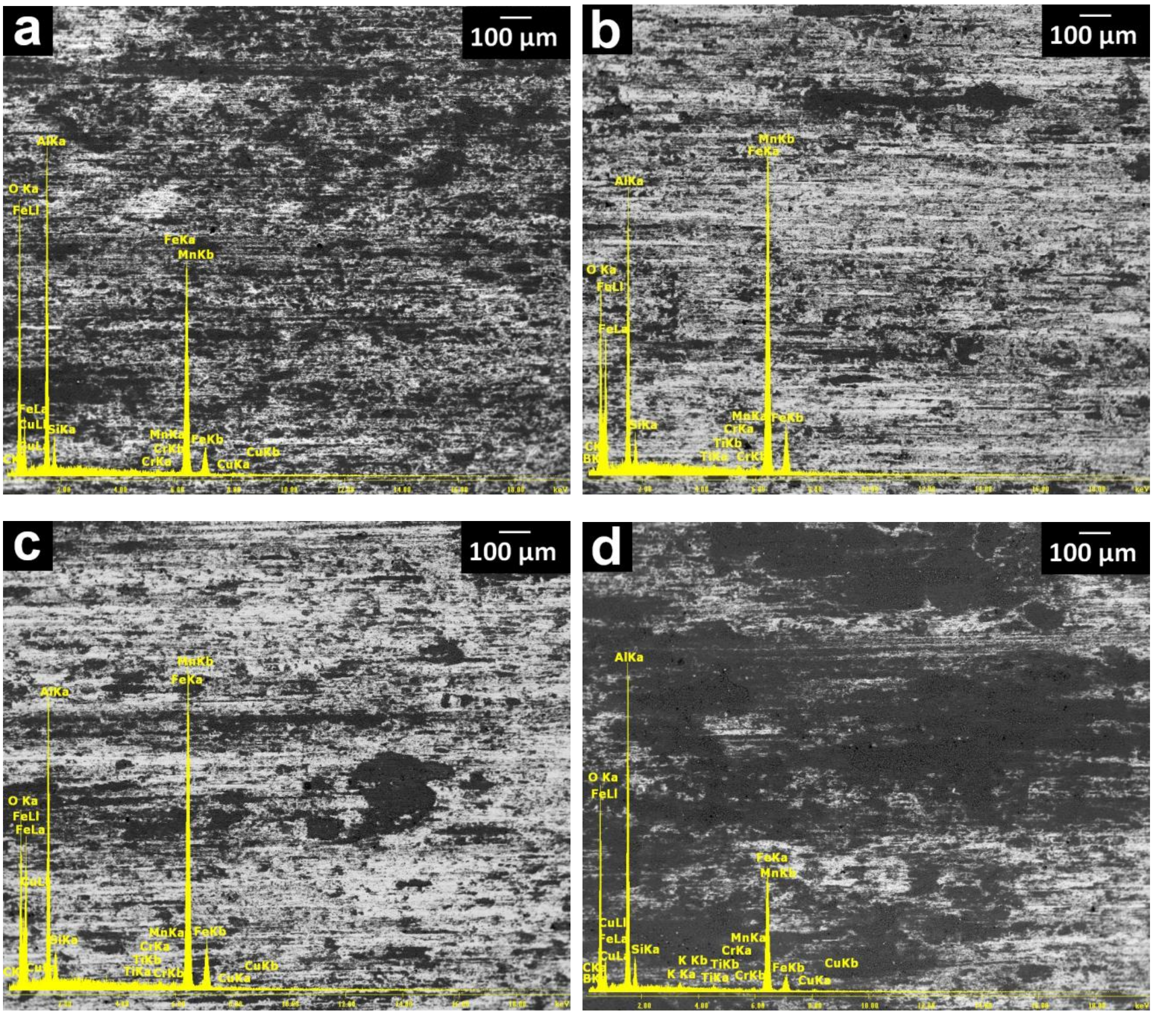

Fig. 13. Low magnification BSI SEM images of the worn surfaces and matching EDS analysis of pins worn against a) 15%, b) 19% reinforced composites in light conditions and c) 15%, d) 19% reinforced composites in harsh conditions

In higher magnification examinations in pins, the worn surfaces showed the following features: (i) craters, (ii) patches and (iii) adhered flakes. Fig. 14 shows the craters on the surface of the pin worn against 19% B_4C reinforced composite in light conditions. Those craters also confirms adhesive wear due to the formation of and breaking of micro welds during sliding, similar to the composite worn surfaces that given in Fig. 9.

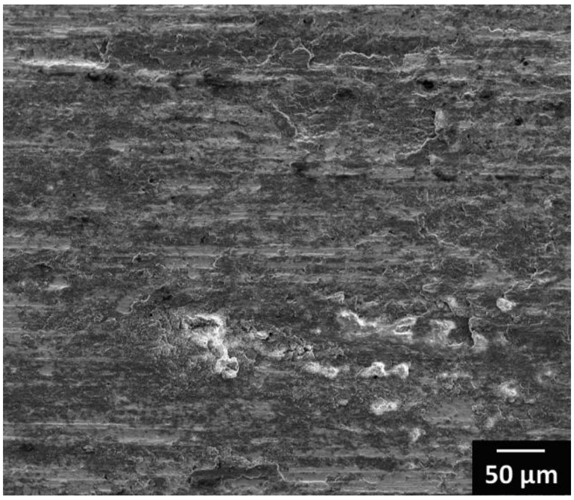

Fig. 14. Craters on SE SEM image of the surface of the pin worn against 19% B_4C reinforced composite in light conditions

Fig. 15 (a) shows an adhered flake on the on the surface of the pin worn against 15% B_4C reinforced composite in harsh conditions. After the EDS analysis taken from those flake (Fig. 15b) it has deduced that this flake detached from the composite sample due to the delamination wear and adhered to the pins surface during the sliding.

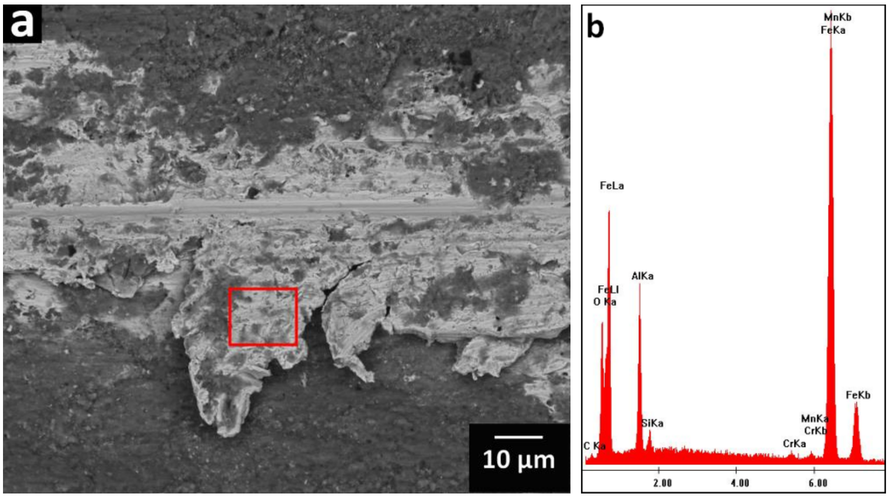

Fig. 15. a) Adhered flake on BSI SEM image of the surface of the pin worn against 15% B_4C reinforced composite in harsh conditions and b) EDS analysis taken from the marked area

Fig. 16 (a) shows the loose and compacted oxidised patches on the surface of the pin worn against 19% B_4C reinforced composite in harsh conditions. EDS analysis taken from the loose and compacted areas are given in Figs. 16 (b) and (c) respectively. It has concluded from the EDS analysis that the patches have the similar composition with the tribolayer.

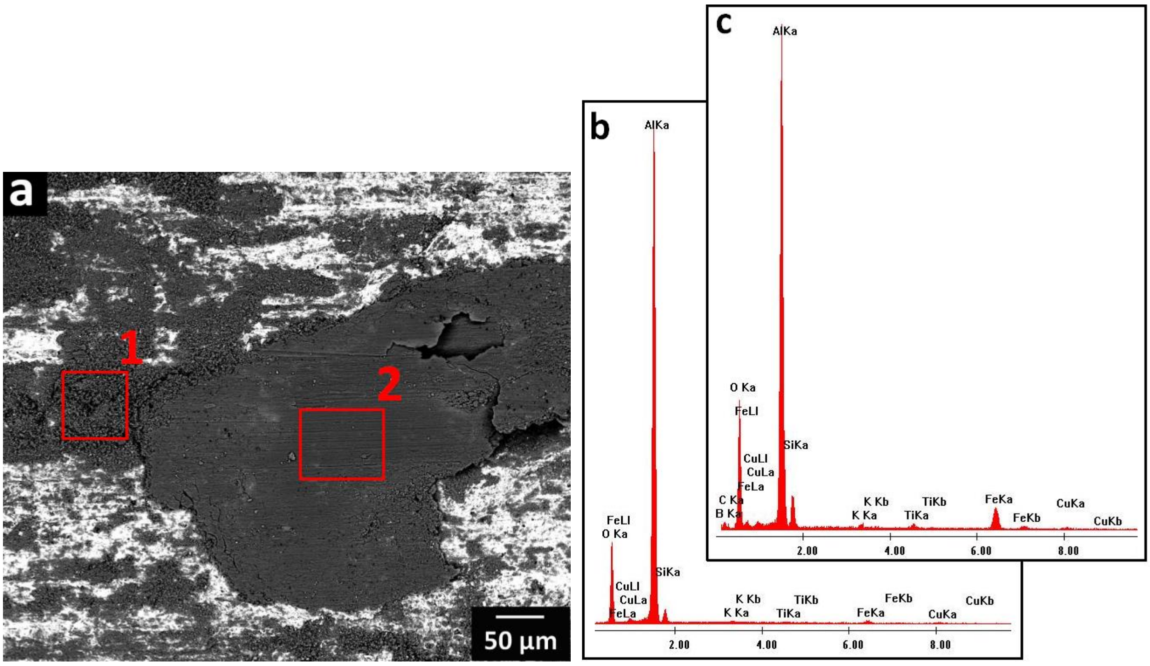

Fig. 16. a) Oxide patches on BSI SEM image of the surface of the pin worn against 19% B_4C reinforced composite in harsh conditions and b and c) EDS analysis taken from "1" and "2" areas indicated in "a"

3.2.7. Wear mechanism

Due to COF graphs and characterisation of wear surfaces, the wear mechanism has been suggested as following: At the initial stage, load is mainly borne by reinforcing particles and it results with relatively lower COF values. As sliding time increases, B_4C particles abrade the counter material. When grooves occurred on the counter materials surface, counter materials surface starts to contact with the aluminium matrix surface. This contact results with the adhesive wear which can be distinguished by craters and adhered flakes in both surfaces and abrasive wear which can be distinguished by grooves in composite surfaces.

Another result of this contact is the forming of mechanically mixed layer which can be detected by elements of counter wear pair and oxides on the wear surfaces. Therefore, while the contact is mainly metal-ceramic at the initial stage, as sliding time increases, the metallic character of the contacting wear surface increases. This situation leads to increasing of COF values during the sliding. On the other hand, due to plastic deformation, cracks starts to nucleate and propagate which causes delamination wear. Therefore, wear mechanism can be suggested as a combination of adhesive, abrasive, and delamination wear.

4. CONCLUSIONS

AlSi9Cu3Mg alloy matrix composites reinforced with 15 and 19% (vol.) B_4C_p were produced by squeeze casting route at 850 °C under low vacuum with addition of titanium-containing flux. The samples were subjected to reciprocating wear tests against AISI 4140 pin under dry sliding conditions. Effects of B_4C volume fraction, sliding velocity, applied load and sliding distance on reciprocal dry wear behaviour of composites were studied using general full factorial experimental design. From data analysis and microstructural investigations, the followings can be concluded:

- Due to the proper production route with K_2TiF_6 addition, relatively homogenous particle distribution, relatively high volume fraction and relatively decreased porosity values obtained.
- From analysing experimental analysis, it can be concluded that;
    - COF and wear rates increased as volume fraction increased
    - COF and wear rates decreased as velocity increased

- COF decreased and wear rates increased as load increased
- COF and wear rates increased as distance increased

- From data analysis, it can be concluded that volume fraction is the most important factor for COF while load is the most important factor for wear rates
- Wear mechanism can be suggested as a combination of adhesive, abrasive, and delamination wear.

Acknowledgements

This study was partially supported by TUBITAK (The Scientific and Technological Research Council of Turkey) under Grant No. 107M338. The authors would also like to thank for their kind help to Prof. Ö. Keleş from Istanbul Technical University for experimental design studies, Prof. A. Ramalho from University of Coimbra for profilometry studies, and Prof. J. Gomes and Mr. S. Carvalho from University of Minho for tribological studies.

References

[1] K. Tokaji, Fatigue Fract Engng Mater Struct 28 (2005) 539–545.

[2] K.B. Lee et al., Metall Mater Trans A 32A (2001) (4), 1007–1018.

[3] I. Kerti and F. Toptan, Mater Lett 62 (2008) 1215–1218.

[4] R. Ipek, J Mater Process Tech 162–163 (2005) 71–75.

[5] F. Bedir, Mater Design 28 (2007) 1238–1244.

[6] A. Kalkanlı and S. Yılmaz, Mater Design 29 (2008) 775–780.

[7] I. Kerti, Mater Lett 59 (2005) 3795–3800.

[8] K.B. Khan et al., Mater Sci Eng A 427 (2006) 76–82.

[9] H. Zhang et al., Mater Sci Eng A 384 (2004) 26-34.

[10] M. Aizenshtein et al., Scripta Mater 53 (2005) 1231–1235.

[11] J. Jung and S. Kang, J Am Ceram Soc 87 [1] (2004) 47–54.

[12] X. Zhu et al., Surf and Coat Tech 202 (2008) 2927–2934.

[13] N.K. Shrestha et al., Surf and Coat Tech 200 (2005) 2414– 2419.

[14] C.A. Smith, Discontinuous Reinforcements for Metal-Matrix Composites, ASM Handbook, Vol. 21, Composites, ASM International, 2001.

[15] Z. Zhang et al., J Mater Sci (2007) 42:7354–7362.

[16] K. M. Shorowordi et al., J Mater Process Tech 142 (2003) 738–743.

[17] F. Toptan et al., Mater Sci Forum 636-637 (2010) 192-197.

[18] F. Toptan et al., Mater Design 31 (2010) S87–S91.

[19] A. Canakci, F. Arslan, Proc. of 11th Int. Mater. Symp., Denizli (2006) 382-389.

[20] J. Hemanth, Wear 258 (2005) 1732–1744.

[21] A. Canakci, F. Arslan, Proc. of 12th Int. Metall. & Mater. Cong., Istanbul (2005), 772-783.

[22] K.M. Shorowordi et al., Wear 261 (2006) 634–641.

[23] K.M. Shorowordi et al., Wear 256 (2004) 1176–1181.

[24] H.R. Lashgari et al., Mater Design 31 (2010) 2187–2195.

[25] H.R. Lashgari et al., Mater Design 31 (2010) 4414–4422.

[26] A. Mazahery and M.O. Shabani, J Mater Eng Perform 21 (2011) 247-252.

[27] A. Canakci, J Mater Sci 46 (2011) 2805–2813.

[28] A. R. Kennedy and B. Brampton, Scripta Mater 44 (2001)1077-1082.

[29] D.C. Halverson et al., J Am Ceram Soc 72 [5] (1989) 775-80.

[30] A.R. Kennedy and A.E. Karantzalis, Mater Sci and Eng A 264 (1999) 122–129.

[31] D.C. Halverson et al., US Patent no. 4,605,440, 1986.

[32] A. R. Kennedy, J Mater Sci 37 (2002) 317– 323.

[33] J. Hashim et al., J Mater Process Tech 92-93 (1999) 1-7.

[34] H. Sevik and S.C. Kurnaz, Mater Design 27 (2006) 676–683.

[35] K. Laden et al., Tribol Lett 8 (2000) 237–247.

[36] Sur et al., J Fac Eng Arch Gazi Univ 20(2) (2005) 233-238.

[37] M. Kök, Fen ve Mühendislik Dergisi 4 (2001) 131-142.

[38] S. Buytoz and H. Eren, Science and Eng J of Fırat Univ 19 (2) (2007) 209-216.

[39] M.R. Rosenberger et al., Wear 259 (2005) 590–601.

[40] F. Tang et al., Wear 264 (2008) 555–561.

[41] O. Meydanoglu et al., Proc. of 11th Int. Mater. Symp., Denizli (2006) 270-272.

[42] H. Mindivan, Mater Lett 64 (2010) 405–407.

[43] G. Akin et al., Proc. of 12th Int. Metall. & Mater. Cong., Istanbul (2005) 735-740.

[44] V.R. Rajeev et al., Tribol Int 43 (2010) 1532–1541.

[45] S. Anoop et al., Mater Design 30 (2009) 3831–3838.

[46] S. Suresha and B.K. Sridhara, Mater Design 31 (2010) 1804–1812.

[47] S. Suresha and B.K. Sridhara, Compos Sci and Technol 70 (2010) 1652–1659.

[48] S. Suresha and B.K. Sridhara, Mater Design 31 (2010) 1804–1812.

[49] S. Suresha and B.K. Sridhara, Mater Design 34 (2012) 576–583.

[50] J.S.S. Babu et al., Mater Design 32 (2011) 3920–3925.

[51] S. Kumar and V.Balasubramanian, Tribol Int 43 (2010) 414–422.

[52] S. Basavarajappa et al., Mater Design 28 (2007) 1393–1398.

[53] Y. Şahin, Tribol Int 43 (2010) 939–943.

[54] S.Basavarajappa and G.Chandramohan, J Mater Sci Technol 21 (2005) 845-850.

[55] Y. Sahin, Mater Design 24 (2003) 95–103.

[56] S. Naher et al., J Mater Process Tech, 166, (2005) 430–439.

[57] P. Shen et al., Mater Sci and Eng A 454–455 (2007) 300–309.

[58] J.P. Davim, J Mater Process Tech 132 (2003) 340-344.

[59] N.A.Shuaib et al., IJET-IJENS 11(01) (2011) 182-187.

[60] R. L. Deuis et al., Compos Sci Technol 57 (1997) 415-435.

Figure Captions

Fig. 1. Back-scattered electron (BSI) SEM images of a) 15% and b) 19% reinforced composites

Fig. 2. a, c) BSI SEM images and b,d) matching Ti elemental maps of 15% and b) 19% reinforced composites respectively

Fig. 3. COF graphs for a) light and b) harsh wear conditions

Fig. 4. a) Normal probability and b) main effect plots for avg. COF

Fig. 5. a) Normal probability and b) main effect plots for wear rate

Fig. 6. Normal probability and b) main effect plots for wear rate in counter material

Fig. 7. Low magnification secondary electron (SE) SEM images of the worn surfaces and matching EDS analysis for a) 15%, b) 19% reinforced composites worn in light conditions and c) 15%, d) 19% reinforced composites worn in harsh conditions

Fig. 8. OM image showing B_4C protrusions on the worn surface of 15% reinforced composite worn in light conditions

Fig. 9. SE SEM image of the craters on the worn surface of 19% B_4C reinforced composite worn in harsh conditions

Fig. 10. a) SE SEM images of a large flaky piece is about to be dislodged from the surface from 15% B_4C reinforced composite worn in light conditions and b) EDS analysis taken from the marked area

Fig. 11. Plastic deformation on a) 15% reinforced composite worn in light conditions and b) cracks on 19% reinforced composite worn in harsh conditions in BSI and SE SEM images, respectively

Fig. 12. a) SE SEM image and b) matching EDS analysis of uncompacted powdery debris from 19% B_4C reinforced composite worn in harsh conditions

Fig. 13. Low magnification BSI SEM images of the worn surfaces and matching EDS analysis of pins worn against a) 15%, b) 19% reinforced composites in light conditions and c) 15%, d) 19% reinforced composites in harsh conditions

Fig. 14. Craters on SE SEM image of the surface of the pin worn against 19% B_4C reinforced composite in light conditions

Fig. 15. a) Adhered flake on BSI SEM image of the surface of the pin worn against 15% B_4C reinforced composite in harsh conditions and b) EDS analysis taken from the marked area

Fig. 16. a) Oxide patches on BSI SEM image of the surface of the pin worn against 19% B_4C reinforced composite in harsh conditions and b and c) EDS analysis taken from “1” and “2” areas indicated in “a”

Table Captions

Table 1. Chemical composition of AlSi9Cu3Mg matrix material

Table 2. Factors and their levels chosen for 2^4 full factorial design

Table 3. Plan of experiments

Table 4. Physical properties and hardness values

Table 5. Experimental plan with results

Table 6. ANOVA table for avg. COF

Table 7. ANOVA table for wear rate

Table 8. ANOVA table for wear rate values in counter material

*Highlights

Highlights

- $AlSi9Cu3Mg-15B_4C$ and $AlSi9Cu3Mg-19B_4C$ composites were produced under low vacuum.
- Homogenous particle distribution, and decreased porosity values were obtained.
- Effects of various parameters on the dry sliding behaviour of composites were studied.
- We find that volume fraction and load are the most important factors for COF and wear rates, respectively.
- We suggested the wear mechanism as a combination of adhesive, abrasive, and delamination wear.